Achieving an Accurate Surface Profile of a Photonic Crystal for Near-Unity Solar Absorption in a Super Thin-Film Architecture

Ping Kuang,[†] Sergey Eyderman,[‡] Mei-Li Hsieh,[§] Anthony Post,[†] Sajeev John,[‡] and Shawn-Yu Lin*,[†]

[†]The Future Chips Constellation and the Department of Physics, Applied Physics, and Astronomy, Rensselaer Polytechnic Institute, 110 Eighth Street, Troy, New York 12180, United States

[‡]Department of Physics, University of Toronto, 60 St. George Street, Toronto, Ontario M5S 1A7, Canada

[§]Department of Photonics, National Chiao-Tung University, Hsinchu, Taiwan 300

S *Supporting Information*

ABSTRACT: In this work, a teepee-like photonic crystal (PC) structure on crystalline silicon (c-Si) is experimentally demonstrated, which fulfills two critical criteria in solar energy harvesting by (i) its Gaussian-type gradient-index profile for excellent antireflection and (ii) near-orthogonal energy flow and vortex-like field concentration *via* the parallel-to-interface refraction effect inside the structure for enhanced light trapping. For the PC structure on 500-μm-thick c-Si, the average reflection is only ~0.7% for λ = 400–1000 nm. For the same structure on a much thinner c-Si (t = 10 μm), the absorption is near unity ($A \sim 99\%$) for visible wavelengths, while the absorption in the weakly absorbing range ($\lambda \sim 1000$ nm) is significantly increased to 79%, comparing to only 6% absorption for a 10-μm-thick planar c-Si. In addition, the average absorption (~94.7%) of the PC structure on 10 μm c-Si for λ = 400–1000 nm is only ~3.8% less than the average absorption (~98.5%) of the PC structure on 500 μm c-Si, while the equivalent silicon solid content is reduced by 50 times. Furthermore, the angular dependence measurements show that the high absorption is sustained over a wide angle range (θ_{inc} = 0–60°) for teepee-like PC structure on both 500 and 10-μm-thick c-Si.

Teepee Photonic Crystal

KEYWORDS: *photonic crystal, antireflection, light trapping, ultrathin silicon, thin-film photovoltaics*
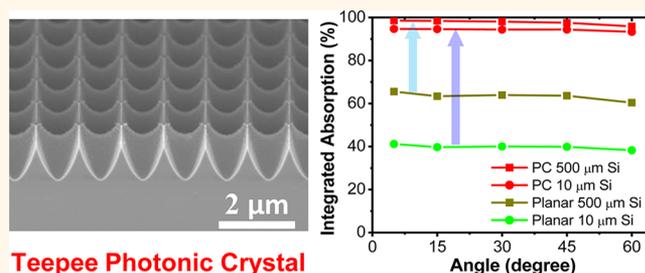
The development and utilization of solar cells and solar power have steadily increased in recent years in the effort to create a sustainable, renewable, clean energy resource. At present, crystalline and multicrystalline silicon (c-Si and m-Si)-based photovoltaics (PVs) are still the largest constituents of worldwide solar cell and module productions. However, the utilization of c-Si solar cells is being hindered by their high dollar-per-Watt cost. In order to retain its competitiveness, the best approach is to develop different silicon PV cell designs which are capable of achieving high energy conversion efficiency while using much less high-quality c-Si material, and the thickness of silicon has to be reduced from hundreds of micrometers to a cost-effective level of tens of micrometers, or even less. Some reports have already experimentally shown that moderate conversion efficiencies have been achieved with ultrathin c-Si solar cells.[1–5] Nevertheless, thinner silicon still has a major disadvantage of insufficient light absorption in the longer near-infrared (IR) range of the solar spectrum, which in turn reduces the efficiency of the solar cell device.

In order to overcome low IR absorption in thin-film solar cells, various schemes of light trapping mechanisms were proposed to (i) reduce the reflection and (ii) enhance light absorption. Both approaches are critical and desirable for performance improvement and cost reduction in solar cells. For reflection reduction, antireflective coating (ARC) designs of nanowires and nanorods,[6–8] moth-eyes,[9] and graded-index multilayer films[10–12] have been extensive studied. Furthermore, textured or patterned nanostructures such as nanowires,[13,14] nanocones,[2,15,16] nanopyramids,[1,17,18] plasmonics,[19] and photonic crystals (PCs)[20–23] all have been extensively investigated for enhanced light trapping and improved absorption in thin-film solar cells. One intriguing optical phenomenon is the parallel-to-interface refraction (PIR) in PCs.[21,24–28] PIR effect is a negative refraction of light inside a PC, producing nearly perpendicular light-bending phenomenon. This acute light-bending phenomenon directly results in increased optical path
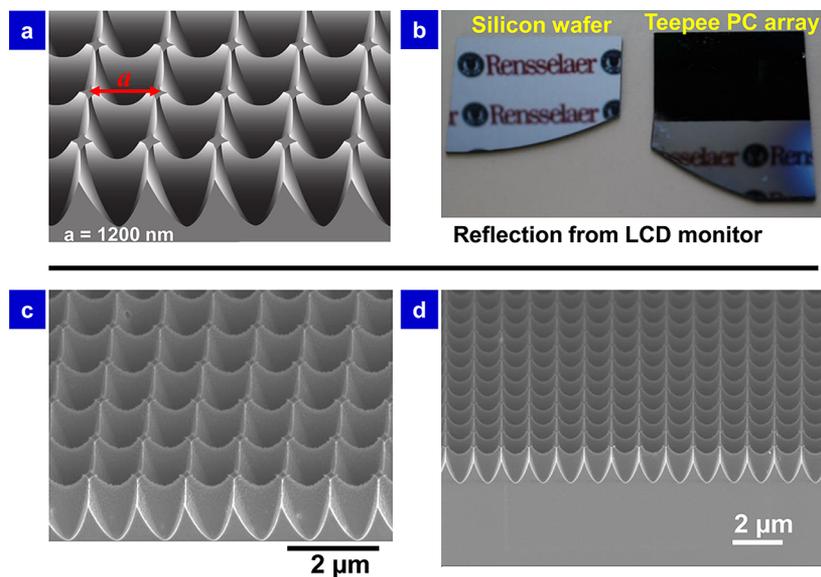
Figure 1. (a) Schematic representation of the teepee-like PC structure. (b) Optical reflection from polished, planar silicon wafer surface and from the teepee-like PC structure surface. (c) SEM image of the teepee-like PC structure at slanted view. (d) SEM image of the PC at front side view.

lengths and exhibits vortex-like circulation patterns inside a structured medium, thus improving light trapping and absorption over a broad wavelength range.[21,24,25] We already have experimentally demonstrated the PIR effect in amorphous silicon (a-Si)-based 3D simple cubic woodpile PCs, which exhibit broadband, wide-angle near-unity absorption.[27]

Here, we report on a teepee-like PC on c-Si which fulfills two critical criteria in solar energy harvesting by (i) its gradient-index profile for antireflection and (ii) parallel-to-interface energy flow and vortex-like field concentration for enhanced light trapping. Hence, such structure offers superior absorption in a much broader visible and near-IR wavelength range, specifically matching the silicon bandgap for maximum solar energy harvesting. To experimentally realize the teepee-like PC, we have developed a unique reactive-ion etching (RIE) dry etching process, which is repeatable and IC-technology compatible for high-throughput, wafer-scale fabrications. We show, for the PC structure on conventional 500-μm-thick c-Si with only one-layer (1L) ultrathin SiO_2 ARC ($t \sim 60$ nm), the minimum reflection (R_{min}) is suppressed to a negligible level of $\sim$0.004%, and the average reflection (R_{avg}) is only $\sim$0.7% for λ = 400−1000 nm. We also show, for the same structure on much thinner c-Si ($t = 10~\mu$m), with the 1L SiO_2 ARC and a 200 nm silver (Ag) back reflector, the absorption is near unity ($A \sim 99\%$) for visible wavelengths, while the absorption is significantly increased to $\sim$79% due to the aforementioned PIR effect in the weakly absorbing, near-IR range ($\lambda \sim 1000$ nm). This is more than 13 times of absorption enhancement when compared to only $\sim$6% absorption for a 10-μm-thick c-Si planar film. We believe this is the highest near-IR absorption reported for 10-μm-thick c-Si to date. For comparison, the average absorption ($A_{avg} \sim 94.7\%$) of the teepee-like PC on 10 μm c-Si for λ = 400−1000 nm is only $\sim$3.8% less than that for the same teepee-like PC on 500 μm c-Si, while the equivalent silicon solid content is reduced by 50 times. Furthermore, the angular dependence measurements show that the high absorption is sustained over a wide angle range ($\theta_{inc} = 0-60°$) for teepee-like PC on both 500 and 10-μm-thick c-Si.

RESULTS AND DISCUSSION

We propose a unique architecture design, namely, teepee-like PC as shown in Figure 1a. The SEM images (Figure 1c, d) reveal the actual structures of the teepee-like PC structure with the simple cubic symmetry[29] at different viewing directions. The periodicity of the PC is $a = 1.2~\mu$m, and the height (h) is 1.4 μm. Figure 1d (low magnification) shows the front view of the structure, which demonstrates a uniform RIE etching results on the silicon surface and preserves a V-shaped, inverse-conical like profile with very high $h/(a/2)$ ratio ($\sim$2.3). The bottom of trenches also is very sharp, with the sidewall angle $\sim$70°. For comparison, The typical inverted pyramid structure profile by KOH etching has a sidewall angle of $\sim$54°, and a $h/(a/2)$ ratio of only $\sim$1.3. Therefore, the teepee-like PC has a greater vertical depth for better light trapping. As shown in Figure 1c, some minor surface roughness is resulted due to the dry etch, which can cause silicon surface degradation and high surface recombination velocity.[30] To overcome this, an ultrathin SiO_2 coating ($t \sim 60$ nm) by high-temperature oxidation and annealing was introduced, which could provide efficient surface passivation as well as excellent antireflection property.[3,31,32] From the optical image in Figure 1b, it is easily seen that the surface reflection for polished silicon wafer surface is noticeably high, while the RPI logo is clearly visible. On the contrary, the reflection of the PC structure with 1L SiO_2 ARC ($t \sim 60$ nm) is substantially reduced. The sample appears to be black, indicating a very high absorption in the c-Si. (The bottom half of the sample silicon area is unpatterned and flat, so the logo is still visible in this area.)

In order to create the teepee PC, a simple standard semiconductor fabrication process is utilized, which can readily achieve the desired surface profile by one-step RIE etching in c-Si. A typical photoresist 2D hole array with simple cubic symmetry (lattice constant $a = 1.2~\mu$m) was made by standard photolithography. Then, RIE etching was carried out with the resist pattern as the etch mask (Figure 2a). Low RIE power was used to avoid excessive silicon etching damage and surface roughness by SF_6 etchants. Different SF_6/CHF_3 ratios were
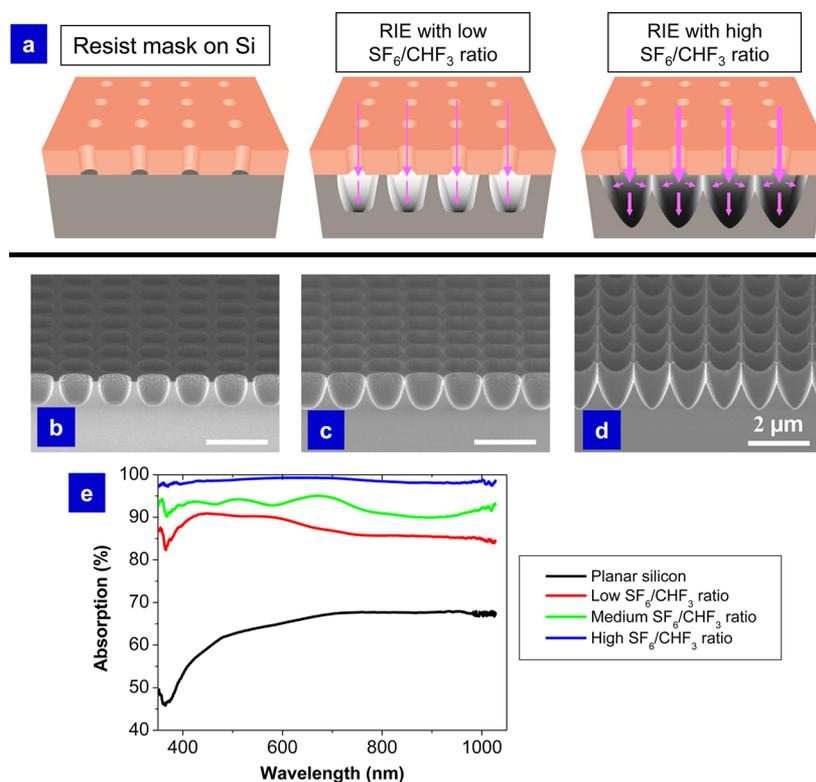
Figure 2. (a) Schematic representation of the PC structure fabrication process. (Dimensions are not to scale.) SEM images (cross-sectional view) of the PC structures fabricated at (b) low SF_6/CHF_3 ratio (ratio = 1:1), (c) medium SF_6/CHF_3 ratio (ratio = 2:1), and (d) high SF_6/CHF_3 ratio (ratio = 3:1), resulting in a teepee-like PC structure. (e) Measured absorption of the four different samples. Black: planar silicon (t = 500 μm), red: RIE with low SF_6/CHF_3 ratio, green: RIE with medium SF_6/CHF_3 ratio, blue: RIE with high SF_6/CHF_3 ratio.

tested and resulted in various surface profiles, while CHF_3 provided passivation for the silicon surface. The low and medium SF_6/CHF_3 ratio etch (ratio = 1:1 and 2:1) inhibits aggressive SF_6 reaction on the sidewalls and promotes slower, anisotropic etching, as shown in Figure 2b,c after resist removal. In contrast, a high SF_6/CHF_3 ratio etch (ratio = 3:1) allows a faster and more isotropic etching in vertical and lateral directions, while the sidewalls still remain relatively smooth due to sufficient CHF_3 passivation. This fast, yet balanced RIE etching ultimately resulted in the V-shaped, inverted-conical-like profile with very high $h/(a/2)$ ratio (Figure 2d). The total absorption of samples (with 60 nm SiO_2 coating) with different SF_6/CHF_3 etching recipes were measured and shown in Figure 2e. The absorption of 500-μm-thick planar silicon was also taken for comparison. It is evident that the RIE etched samples have much higher absorption than that of the planar silicon, which has an A_{avg} of 65.5% in the wavelength range λ = 400–1000 nm. Moreover, as the SF_6/CHF_3 ratio increases, the absorption is also increased. For low SF_6/CHF_3 ratio etch, the A_{avg} is 87.2%, while A_{avg} of the medium SF_6/CHF_3 ratio etched sample is improved to 92.4%. The A_{avg} is further improved, ultimately reaching near unity (98.5%) for the teepee-like PC structure achieved by the high SF_6/CHF_3 ratio etching.

It is well-known that subwavelength nanostructures, such as nanowires and nanorods, with effectively graded refractive index profiles at the air−silicon interface exhibit excellent antireflection properties.[7−9,15] These structural designs provide superior antireflection with suppressed reflection over wide wavelength and angular range than traditional quarter-wavelength thin-film AR coatings. Minfeng Chen et al.[33] introduced a selection principle for gradient-index ARC designs, of which a

Gaussian-type profile with smooth and uniform refractive angle change (*i.e.*, optical path change in the material) gives the optimal wide-angle AR performance.[33] The expression for the Gaussian-type profile takes the general form of

$$n(x) = n_{\min} + (n_{\max} - n_{\min})e^{-(x-1/b)^2} \quad (1)$$

where $n_{\min}$ and $n_{\max}$ are the minimum and maximum refractive index, respectively, x is the normalized optical distance, and b = ~0.52 $\pm$ 0.02, which represents the profile shape width.

By discretizing the cross section in the middle of our teepee-like PC structure (Figure 3d) and estimating the solid (volume) fraction of the silicon structure at each discretized level, we were able to calculate the effective refractive index, $n(z)$, using effective volume filling ratio at different physical thickness, z, which is proportional to the optical distance. (Optical constants of silicon were taken from elsewhere.)[34] Figure 3a−c is the plot of the effective refractive indexes and their respective Gaussian fits at wavelengths λ = 400, 600, and 800 nm, respectively. It shows that $n(z)$ of PC structure varies gradually along the normalized physical thickness and the variation can be closely fitted to the Gaussian-type profile (Figure 3e). Therefore, when lights impinge onto the sharp-angle sidewalls of the air−silicon interface, they have large incident angles and are refracted smoothly into the PC. This significantly reduces the backward reflection commonly observed at interfaces with abrupt index change, and we expect it will have excellent antireflection performance.

To validate the gradient-index AR effect, we carried out total reflection measurements using unpolarized light source for c-Si-based teepee-like PC samples with two different thicknesses (t = 500 and 10 μm). Figure 4a shows the total reflection spectra
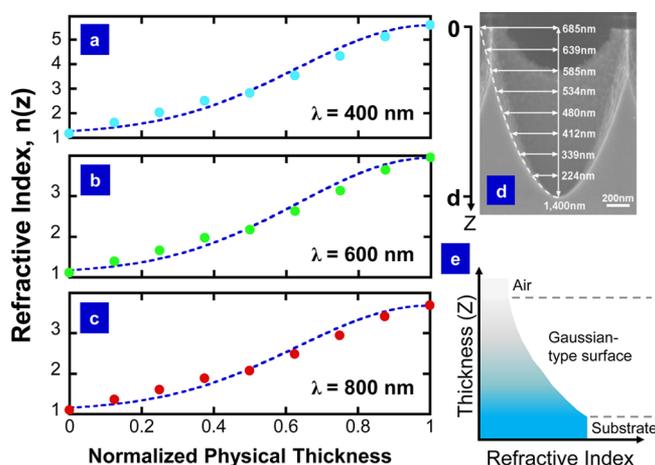
Figure 3. Effective refractive index $n(z)$ of teepee-like PC silicon structure and the Gaussian fit (blue curves) of the refractive index at wavelength (a) $\lambda = 400$ nm, (b) $\lambda = 600$ nm, and (c) $\lambda = 800$ nm. (d) SEM image shows the Gaussian-type profile of the teepee PC and widths used to calculate $n(z)$. (e) The schematic representation of the refractive index profile of the teepee PC Gaussian-type surface.
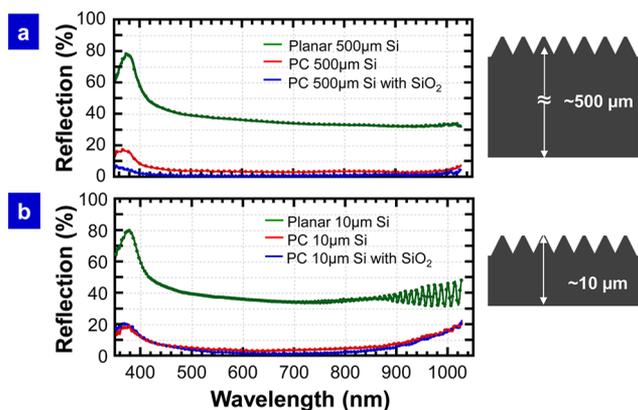

Figure 4. (a) Total reflection of 500-μm-thick planar silicon (green), teepee-like PC structure on 500-μm-thick silicon (red), and teepee-like PC structure on 500-μm-thick silicon with 60 nm SiO$_2$ AR coating (blue). (b) Total reflection of 10-μm-thick planar silicon (green), teepee-like PC structure on 10-μm-thick silicon (red), and teepee-like PC structure on 10-μm-thick silicon with 60 nm SiO$_2$ AR coating (blue).

for 500-μm-thick c-Si PC samples, while Figure 4b shows the spectra for 10-μm-thick samples. For comparison, the reflections of flat, polished c-Si films of respective thicknesses were also measured. As anticipated, in Figure 4a, the average reflection of the 500-μm-thick, planar c-Si is ~35.5% in the visible and near-IR wavelength range [$\lambda = 400-1000$ nm]. For the teepee-like PC structure produced by RIE etching on 500-μm-thick c-Si, the reflection is drastically reduced in the same wavelength range. The average reflection is only ~3.4% for $\lambda = 400-1000$ nm, with a minimum reflection of ~2.5% at $\lambda \approx 920$ nm. Such significant reflection reduction is directly attributed to the graded index profile of the teepee-like PC structure at the surface of the c-Si. This shows that our unique PC structure itself already possesses a broadband, antireflection property due to the gradient-index, Gaussian-type profile even without additional antireflection coatings. However, one can anticipate further improvement if an index-matching oxide layer (e.g.,

SiO$_2$, ZnO, or Al$_2$O$_3$, etc.) is present on the c-Si surface of the structure. To demonstrate, an ultrathin layer of SiO$_2$ (~60 nm) was grown conformally by thermal oxidation on the surface of the PC structure, and additional reduction in reflection was observed. R_{min} is suppressed to a negligible level of ~0.004% at $\lambda \approx 545$ nm, and the R_{avg} is only ~0.7% over the entire wavelength range of $\lambda = 400-1000$ nm. The additional reduction in reflection is the result of index matching at the silicon–air interface by the ultrathin SiO$_2$ coating, which also can serve as a good passivation layer for mitigating surface recombination speed.[31,32] Our PC c-Si structure with only one layer of ultrathin SiO$_2$ AR coating is much simpler and has superior AR performance than the traditional graded index multilayer AR coatings, which generally require 5–7 layers of oxide films with a total thickness of >1 μm.[10,11] To our knowledge, the ultralow reflection of our structure is only rivaled by that of the recent "black silicon solar cell" with 20 nm Al$_2$O$_3$ AR coating by atomic layer deposition deposition.[35] However, our process approach may have potential economic competitiveness advantages. Therefore, our teepee-like PC design offers another route for conventional c-Si solar cell applications with such ultralow reflection, which is also broad angle, as we will discuss in a later section.

Furthermore, in Figure 4b, reflection spectrum of the 10-μm-thick, planar c-Si is almost identical to that of the 500-μm-thick, planar c-Si, and the R_{avg} is ~37.3% in the visible and near-IR wavelength range [$\lambda = 400-1000$ nm]. The slight increase of reflection and the Fabry–Perot interference pattern in the near-IR wavelength region are due to the backside of the 10-μm-thick silicon. Increased reflection at this wavelength range was also observed in the PC on 10-μm-thick silicon samples. For the teepee-like PC structure on 10-μm c-Si, the reflection is also significantly reduced in the same visible and near-IR wavelength range. The R_{avg} is only ~5.9%, with an R_{min} of ~2.8% at $\lambda \approx 630$ nm. With 60 nm SiO$_2$ coating, the R_{min} is decreased to ~0.8% at $\lambda \approx 670$ nm, and the R_{avg} is only ~4.1% over the entire wavelength range of $\lambda = 400-1000$ nm. The average reflection in the main portion of the spectrum ($\lambda = 450-900$ nm) is still at an impressive ~2.2%. Again, as in the planar film case, the average reflection continuously increases in the longer wavelength range and is mostly due to the backside of the 10-μm-thick silicon, with a maximum reflection of ~15.2% at $\lambda \sim 1000$ nm. Nevertheless, the relatively low reflection in near-IR region can provide a different pathway for producing high-efficiency c-Si thin-film solar cells with much lower cost due to much smaller thickness ($t \sim 10$ μm) of the structure comparing to conventional c-Si devices.

Moreover, in order to achieve enhanced light trapping in thin c-Si ($t = 10$ μm), especially for longer wavelength light, it is critical to induce increased optical density of states *via* multitude of resonance modes inside a spatially engineered structure. The aforementioned PIR effect in PCs meets such a requirement. To gain better insights of the PIR light trapping mechanism, the total absorption measurements using unpolarized light source at near-normal incidence ($\theta_{inc} = 5°$) (see Methods section) were taken for the teepee-like PC structure on 10-μm-thick c-Si with a 60 nm ultrathin SiO$_2$ ARC layer and 200 nm Ag back reflector (Figure 5a). The use of low-loss silver back reflector is to eliminate transmission and to have stronger coupling of longer-wavelength incident light to PIR resonance modes formed by the teepee-like PC while minimizing unnecessary absorption in the metal.[36] For comparison, the calculated absorption for PC-based structure was also obtained
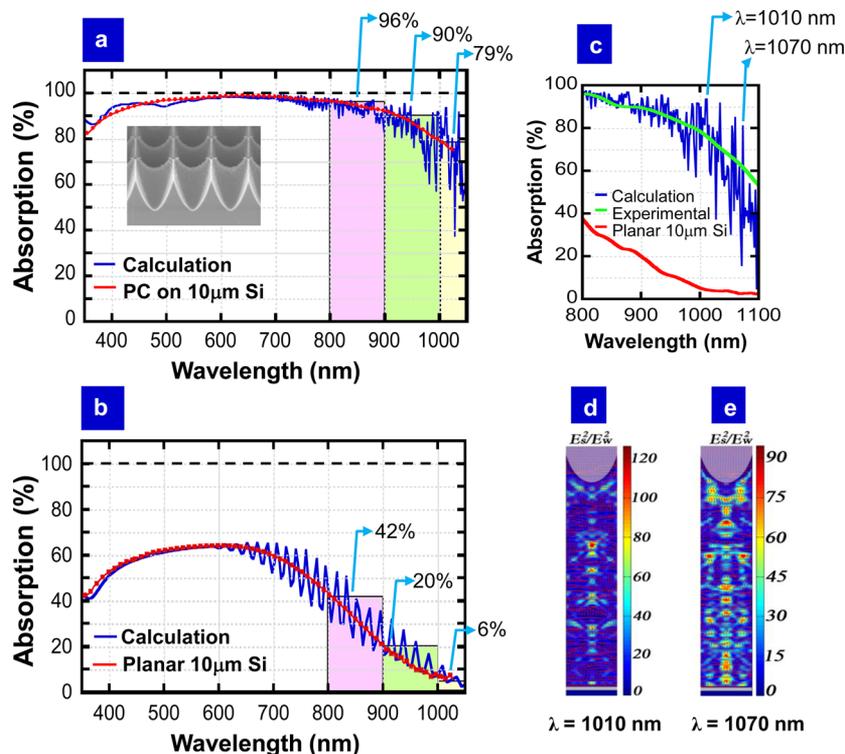
Figure 5. (a) Measured (red) and calculated (blue) total absorption of teepee-like PC on 10-μm-thick silicon. (b) Measured (red) and calculated (blue) total absorption of 10-μm-thick planar silicon. (c) Measured (green) and calculated (blue) near-IR absorption of teepee-like PC on 10-μm-thick silicon and absorption of 10-μm-thick planar silicon (red). Orthogonal slice for resonances at (d) $\lambda = 1010$ nm and (e) $\lambda = 1070$ nm for Poynting vector and energy density distribution show vortex-like, high field concentration (red color regions) in a 10 μm PC silicon film with sunlight impinging from the top.

by finite-difference time-domain (FDTD) simulation with the optical constants retrieved from elsewhere,[37] and it agrees with the measurement results very well. The slight absorption dip in the near-UV region ($\lambda \sim 370$ nm) is mainly due to the higher reflection from higher refractive index of silicon. In the visible and near-IR wavelength range, measured absorption spectrum for the teepee-like PC on 10-μm c-Si structure (PC on 10 μm Si, red curve in Figure 5a) shows that a broad, high absorption is maintained with an A_{avg} of $\sim$94.7% for $\lambda = 400-1000$ nm, while the maximum absorption is close to unity ($A_{max} \sim 99.0\%$) at $\lambda \sim 650$ nm. The calculated absorption (blue curve) of PC-based structure in longer wavelength range shows many distinctive sharp absorption peaks, which are attributed to the PIR effect with near 90° light bending and vortex-like energy flow and circulation patterns. Also, smoothing the calculated absorption peaks in the near-IR spectral range ($\lambda = 800-1000$ nm) shows a similar, sustained high absorption ($A_{cal} \sim 89.2\%$) as the measured absorption ($A_{meas} \sim 90.5\%$), indicating the overall enhanced absorption due to PIR effect shown in simulation is also observed in the measurements. For comparison, the measured and calculated absorptions for a planar 10-μm-thick c-Si flat film are shown in Figure 5b. Without any ARC and metallic back reflector, the planar 10 μm Si sample has a maximum absorption $A_{max} \sim 64.1\%$ at $\lambda \sim 600$ nm. The calculated absorption curve is similar to the measurement except the Fabry–Perot resonances for λs > $\sim$600 nm. As expected, the measured absorption curve exhibits a diminishing trend at longer wavelengths due to the weakly absorbing nature of the silicon material near its bandgap edge. The measured absorption is only $\sim$42%, $\sim$20%, and $\sim$6% at $\lambda =$ 800, 900, and 1000 nm, respectively, in the near-IR region. For

the PC on 10 μm Si structure, the absorptions at the same wavelengths are $\sim$96%, $\sim$90%, and $\sim$79%, respectively. Comparing to the planar silicon film of same thickness, the teepee-like PC structure can enhance the absorption by as much as $\sim$2.3, $\sim$4.5, and $\sim$13 times. The absorption enhancement is the direct result of enhanced light trapping *via* the PIR effect. Also, to our knowledge, the 79% absorption at $\lambda = 1000$ nm is the highest absorption achieved for 10-μm-thick c-Si. Therefore, a significant amount of solar irradiance (visible and near-IR) can be harnessed by the PC structure using only 10 μm of silicon (only $\sim$2% compared to standard 500-μm c-Si). This shows the promise of our teepee-like PC structure for improving the solar energy collection and performance in thin-film c-Si solar cells.

In order to better illustrate the PIR effect in the teepee-like PC, a different experimental setup was used to measure the absorption in the weakly absorbing region (see Methods). Figure 5c shows the absorption plot in the near-IR wavelength range ($\lambda = 800-1100$ nm). The absorption curve of the PC 10 μm structure is in strong agreement with the measured absorption in Figure 5a for $\lambda = 800-1000$ nm. In addition, for $\lambda = 1000-1100$ nm, the absorption is sustained $\sim$53%. For comparison, the measured absorption of a planar 10 μm Si slab approaches $\sim$0% in the same wavelength range. Furthermore, Figure 5d,e depicts the orthogonal slice plots generated by FDTD simulation for Poynting vector and the energy density distribution in the PC 10 μm silicon structure for PIR resonances at $\lambda \sim 1010$ nm and $\lambda \sim 1070$ nm, which correspond to two sharp peaks in the calculation curve in Figure 5c. The plots show that the energy flow exhibits circulation in certain areas in addition to overall "parallel-to-
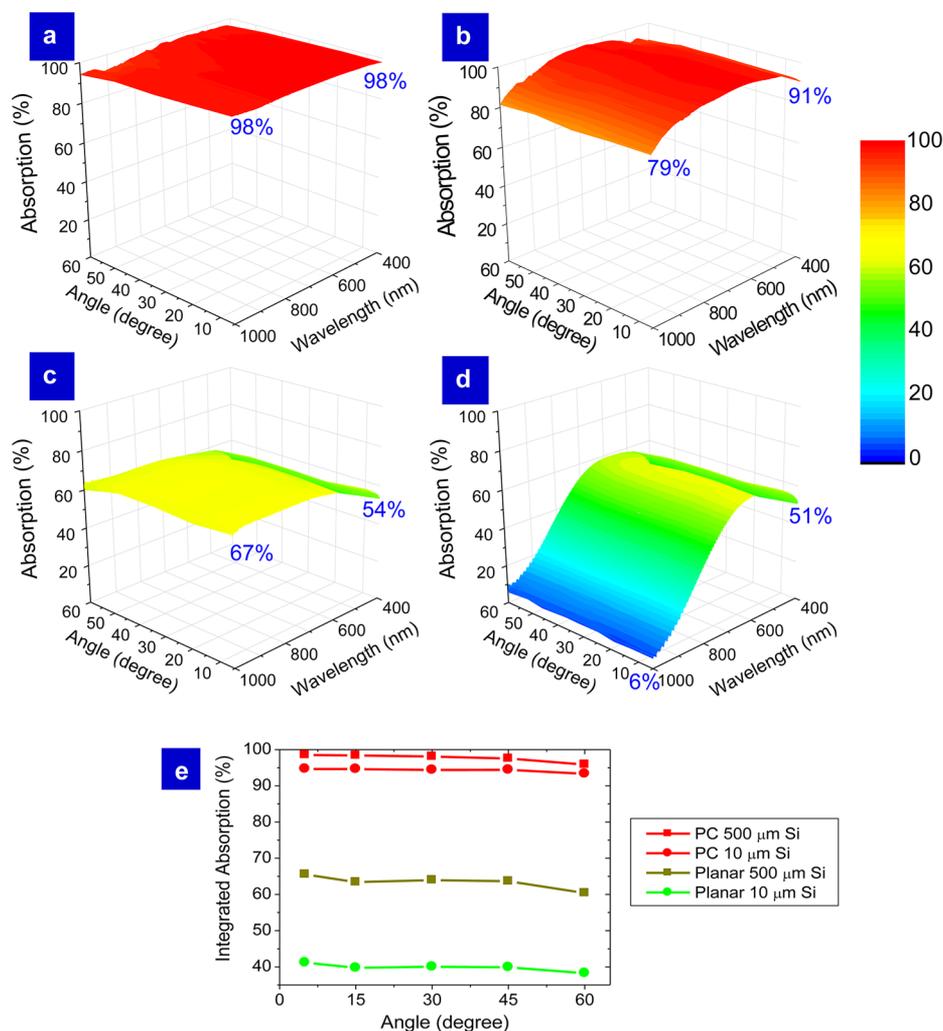
Figure 6. 3D contour plots of measured total absorption of (a) teepee-like PC structure on 500-μm-thick silicon with 60 nm SiO$_2$ AR coating, (b) teepee-like PC on 10-μm-thick silicon with 60 nm SiO$_2$ AR coating and 200 nm Ag back reflector, (c) planar 500-μm-thick silicon, and (d) planar 10-μm-thick silicon at different incident angles. (e) Measured integrated absorption of the four samples for λ = 400−1000 nm at different incident angles.

interface flow". Gray area at the top indicates elliptical nanopores filled with air. The overall depth of nanopores is 1.4 μm, lattice constant is 1.2 μm, ellipse top radius is 0.72 μm, bulk thickness of silicon is 10 μm, and the thickness of silver substrate is 200 nm. A 60 nm thick SiO$_2$ (n = 1.45) is conformally placed on the surface of nanopores. The color bar on the right-hand side indicates a ratio E_s^2/E_w^2, where E_s and E_w are electric fields in the structure and in the incoming plane wave, respectively. These fields are obtained during the numerical experiment and transformed to the frequency domain. A factor of more than 120 intensity enhancement is apparent in specific hot spots for $\lambda \sim 1010$ nm. Similarly, a factor of more than 90 intensity enhancement is shown in specific hot spots at $\lambda \sim 1070$ nm. While optimal antireflection at the top surface of a solar cell is crucial to its performance, light trapping below the surface is important for those wavelength where the intrinsic absorption length scale is long compared to the film thickness. The plot reveals that the light trapping in our structure occurs through the energy flow parallel to the air−silicon interface but strongly augmented by circulation in certain areas (detailed plot see Figure S2). The energy density distribution shows high-intensity peaks mostly

concentrated in the central region where the Poynting vector exhibits vortex-like circulation patterns. This circulation and almost parallel-to-interface energy flow enhance the dwell time of light in the cell, leading to a substantial absorption increase in the near-infrared region where the intrinsic absorption of silicon is weak.[24,25,28]

The unique characteristic of PIR effect in PCs is its ability to achieve high absorption over broad angles. We show the angular response for the teepee-like PC structures (on 500 and 10 μm c-Si) as well as for the 500 and 10 μm planar c-Si. The results are depicted in 3D contour plots in Figure 6a−d for incident angle θ_{inc} = 5−60°. For PC 500 μm Si sample, only a 60 nm SiO$_2$ ARC layer was used. (We assume no transmission for the 500 μm c-Si.) At θ_{inc} = 5°, the absorption is at ~97.3−99.2% for λ = 400−1000 nm, with an $A_{avg} \sim 98.5\%$ (Figure 6a). This is mainly attributed to the exceptional antireflection property of the gradient-index Gaussian-type profile of the teepee-like PC at the air−silicon interface. Furthermore, it is evident that the absorption of PC 500 μm Si at λ = 400−1000 nm is sustained at the same level for incident angles up to θ_{inc} = 45°, at which the A_{avg} is ~97.5%. At θ_{inc} = 60°, there is a slight decrease in absorption around λ = 800−900 nm, but the overall

average absorption is still ~95.9% for λ = 400−1000 nm. On the contrary, the A_{avg} of 500 μm planar c-Si is only 65.5% at θ_{inc} = 5° and is further reduced to 60.4% at θ_{inc} = 60° (Figure 6c). Therefore, the broadband, broad-angle near-100% absorption by the PC 500 μm c-Si with only a 60 nm SiO$_2$ ARC can provide a unique, yet simple, architecture for highly efficient solar energy harvesting in conventional c-Si solar cell applications.

Furthermore, Figure 6b shows the total absorption results of the teepee-like PC on 10 μm c-Si + 1L SiO$_2$ ARC + 200 nm Ag structure for incident angle θ_{inc} = 5−60°. For θ_{inc} = 5°, as discussed before, a broad, high absorption is maintained with an A_{avg} of ~94.7% for λ = 400−1000 nm, while the maximum absorption is close to unity (A_{max} ~ 99.0%) at λ ~ 650 nm. For other higher incident angles, no noticeable decrease in absorption is observed except for θ_{inc} = 60°, where two slight dips are observed at λ ~ 500 nm and λ ~ 900 nm. Nevertheless, the average absorption is still ~93.3%. For near-IR wavelength range λ = 800−1000 nm, the absorption decrease is mainly due to the back reflection from the silicon−silver interface. Still, the absorption remains unchanged for θ_{inc} = 5−45° and is only reduced slightly to ~77.8% for λ ~ 1000 nm at θ_{inc} = 60°. This shows that the high near-IR absorption is the direct result of PIR effect in the PC 10 μm structure, which is insensitive to the change of incident light angles.[24,28] For comparison, the A_{avg} of 10 μm planar c-Si is only 41.2% at θ_{inc} = 5° and is further reduced to 38.3% at θ_{inc} = 60° (Figure 6d).

More importantly, it should be emphasized that, at near-normal incidence for λ = 400−1000 nm, the A_{avg} (~94.7%) of the teepee-like PC structure on 10 μm c-Si is only ~3.8% less than the A_{avg} (~98.5%) of the teepee-like PC structure on 500 μm c-Si (Figure 6e), while the equivalent silicon solid content is reduced by 50 times! Therefore, with only 2% of silicon (10 μm/500 μm), the 10-μm c-Si teepee-like PC has almost the same solar absorption efficiency as the 500-μm c-Si structure. Furthermore, the A_{avg} of the teepee-like PC structure on 500 μm c-Si has decreased ~2.6% at θ_{inc} = 60°, while the A_{avg} of the teepee-like PC structure on 10 μm c-Si has only decreased ~1.3%. This indicates that the teepee-like PC is actually more effective and efficient in much thinner silicon for light trapping purposes. In addition, based on the near-normal incidence absorption results, the calculated maximum achievable photo-current density (MAPD)[38] for the teepee-like PC structure on 10 and 500 μm silicon thicknesses are 34.8 and 36.2 mA/cm^2 for λ = 400−1000 nm, respectively, which are very close to the maximum MAPD (assuming A_{avg} = 100%) of 36.7 mA/cm^2 for the same wavelength range. This again shows that only ~2% of silicon with the 10 μm PC structure is needed for near-maximum photocurrent density generation. In addition, the reduced silicon absorbing layer thickness can be advantageous with possible increased open-circuit voltage (V_{oc}).[39] Therefore, our teepee-like PC shows great potential for thin-film c-Si solar cells applications.

CONCLUSION

In summary, we proposed and demonstrated a unique teepee-like PC design with broadband, wide-angle near-unity solar energy absorption, which is achieved by two light trapping mechanisms: (i) Gaussian-type gradient-index interface profile and (ii) near-orthogonal parallel-to-interface negative refraction. The teepee-like PC structure is realized by a unique but simple photolithography patterning and RIE dry etching process, which is repeatable and IC-technology compatible

for large-area, high-throughput wafer-scale fabrications. The funnel-like geometry of the PC structure with greater vertical depth and higher sidewall angle means it can achieve better light trapping than typical KOH-etched inverted pyramid structures. Teepee-like PC on 500-μm c-Si can already achieve a broadband near-zero reflection and near-unity absorption (A = 98.5%) in λ = 400−1000 nm. For teepee-like PC on much thinner c-Si (t = 10 μm), the average absorption is ~94.7%. Even for near-IR wavelengths (λ = 800−1000 nm), the average absorption is sustained at ~90.5%. The main reason for enhanced light trapping and significantly improved near-IR absorption in much thinner c-Si is the PIR effect, which creates near-90° optical refraction and vortex-like energy circulation patterns concentrated inside absorbing material. Therefore, the teepee-like PC shows excellent promise for achieving greater efficiency improvement in both conventional and thin-film c-Si solar cells toward the Shockley−Queisser limit.[40]

METHODS

Teepee Photonic Crystal Fabrication. Samples were fabricated on either standard 100 mm p-type (ρ = 1−5 Ω cm) 500-μm-thick silicon wafer or 100 mm SOI wafers (vendor: Ultrasil; device layer: 10 μm thick, p-type, ρ = 0.6−0.85 Ω cm; buried oxide layer: 250 nm thick; handle layer: 500 μm thick, p-type, ρ = 1−5 Ω cm) using standard photolithography and RIE dry etching processes. Standard RCA MOS clean was carried out at 70 °C for 10 min each for the silicon wafers, and HF 49% dip is done for 20 s to remove the native oxide. After cleaning, DUV photoresists (UV1400, t ~ 1.2 μm) were spin-coated on wafers by Gamma Automatic Coat-Develop Tool. Photoresist exposure and patterning were done with ASML DUV stepper to achieve square lattice circular holes (a = 1.2 μm, d = 0.3 μm). Exposed photoresist is removed by 726-MIF developer. Standard RIE etching (Oxford PlasmaLab 80+ RIE System) with SF$_6$/CHF$_3$/O$_2$ gas mixture was used for silicon etch. RIE power was kept relatively low at 50 W. Isotropic etching with undercut is resulted from the aggressive SF$_6$ etchant, and CHF$_3$ creates a passivation layer to slow down the etching and balance the over etching at the undercut region. Excess photoresist remained after etching was completely removed by O$_2$ plasma. Silicon dioxide (SiO$_2$) layer was created by wet oxidation in a MRL Industries tube furnace at 900 °C for 20 min and then annealed for 10 min at the same temperature. The thickness of SiO$_2$ was characterized on a planar reference silicon piece using the FilMetrics (F50-EXR) optical measurement system. SOI backside handle layer removal: Silicon nitride (S$_3$N$_4$) was grown by LPCVD as the etch mask on the backside of SOI wafers first, then 12 × 10 mm rectangular opening areas were patterned at the backside with UV1400 photoresist. S$_3$N$_4$ in the opening areas was etched by RIE with CHF$_3$/O$_2$ recipe to expose the handle layer silicon. KOH (30%) wet etch was done at 80 °C for ~6 h. The teepee PC on device layer was covered by an alkaline protective coating (ProTek-B3) for etch protection during KOH etch.

Sample Optical Characterization. Total reflection and absorption measurements were performed using an integrating sphere (Labsphere) with an unpolarized xenon or tungsten-halogen light source. Ocean Optics 2000+ spectrometer was used for data collection. Reflection measurements were taken by placing the samples at the back of the integrating sphere, which collects the total reflected light. The samples were aligned at an 8° angle in order to avoid the specular reflection escaping through the front aperture. The sample was inserted in the middle of the sphere, and the absorption (A) was measured. For angular dependence measurements, the sample holder was rotated accordingly with respect to the incident light beam. The absorption at normal incidence (0°) was neglected because the specular reflection from the sample surface would escape from the integrating sphere. For near-IR wavelength range absorption measurements, Acton SpectraPro SP-2300i monochromator system (Princeton Instruments) was used for data collection with either a high-quality silicon detector or a thermoelectric-cooled InGaAs detector.

ASSOCIATED CONTENT

Ⓢ Supporting Information

The Supporting Information is available free of charge on the ACS Publications website at DOI: 10.1021/acsnano.6b01875.

Dependence of absorption on the periodicity of teepee-like PCs. Dependence of MAPD on the periodicity of teepee-like PCs. Orthogonal slice for resonance at $\lambda = 1070$ nm of the zoomed-in, high-resolution section of the energy density distribution plot showing the close-up of the high field concentration regions. AFM characterizations of flat silicon with or without RIE etching. EDS analysis of teepee PC structure with RIE etching (PDF)

AUTHOR INFORMATION

Corresponding Author

*E-mail: sylin@rpi.edu.

Notes

The authors declare no competing financial interest.

REFERENCES

(1) Branham, M. S.; Hsu, W.; Yerci, S.; Loomis, J.; Boriskina, S. V.; Hoard, B. R.; Han, S.; Chen, G. 15.7% Efficient 10-μm-Thick Crystalline Silicon Solar Cells Using Periodic Nanostructures. *Adv. Mater.* **2015**, *27*, 2182−2188.

(2) Jeong, S.; McGehee, M. D.; Cui, Y. All-back-contact Ultra-thin Silicon Nanocone Solar Cells with 13.7% Power Conversion Efficiency. *Nat. Commun.* **2013**, *4*, 2950.

(3) Seo, K.; Yu, Y. J.; Duane, P.; Zhu, W.; Park, H.; Wober, M.; Crozier, K. B. Si Microwire Solar Cells: Improved Efficiency with a Conformal SiO₂ Layer. *ACS Nano* **2013**, *7*, 5539−5545.

(4) He, J.; Gao, P.; Liao, M.; Yang, X.; Ying, Z.; Zhou, S.; Ye, J.; Cui, Y. Realization of 13.6% Efficiency on 20 μm Thick Si/organic Hybrid Heterojunction Solar Cells via Advanced Nanotexturing and Surface Recombination Suppression. *ACS Nano* **2015**, *9*, 6522−6531.

(5) Yoon, J.; Baca, A. J.; Park, S.; Elvikis, P.; Geddes, J. B.; Li, L.; Kim, R.; Xiao, J.; Wang, S.; Kim, T.; Motala, M. J.; Ahn, B. Y.; Duoss, E. B.; Lewis, J. A.; Nuzzo, R. G.; Ferreira, P. M.; Huang, Y.; Rockett, A.; Rogers, J. A. Ultrathin Silicon Solar Microcells for Semitransparent, Mechanically Flexible and Microconcentrator Module Designs. *Nat. Mater.* **2008**, *7*, 907−915.

(6) Tsai, S. H.; Chang, H. C.; Wang, H. H.; Chen, S. Y.; Lin, C. A.; Chen, S. A.; Chueh, Y. L.; He, J. H. Significant Efficiency Enhancement of Hybrid Solar Cells Using Core−shell Nanowire Geometry for Energy Harvesting. *ACS Nano* **2011**, *5*, 9501−9510.

(7) Park, K. C.; Choi, H. J.; Chang, C. H.; Cohen, R. E.; McKinley, G. H.; Barbastathis, G. Nanotextured Silica Surfaces with Robust Superhydrophobicity and Omnidirectional Broadband Supertransmissivity. *ACS Nano* **2012**, *6*, 3789−3799.

(8) van de Groep, J.; Spinelli, P.; Polman, A. Single-Step Soft-Imprinted Large-Area Nanopatterned Antireflection Coating. *Nano Lett.* **2015**, *15*, 4223−4228.

(9) Sun, C. H.; Jiang, P.; Jiang, B. Broadband moth-eye antireflection coatings on silicon. *Appl. Phys. Lett.* **2008**, *92*, 061112.

(10) Xi, J.-Q.; Schubert, M. F.; Kim, J. K.; Schubert, E. F.; Chen, M.; Lin, S.-Y.; Liu, W.; Smart, J. A. Optical Thin-film Materials with Low Refractive Index for Broadband Elimination of Fresnel Reflection. *Nat. Photonics* **2007**, *1*, 176−179.

(11) Kuo, M. L.; Poxson, D. J.; Kim, Y. S.; Mont, F. W.; Kim, J. K.; Schubert, E. F.; Lin, S. Y. Realization of a near-perfect antireflection coating for silicon solar energy utilization. *Opt. Lett.* **2008**, *33*, 2527−2529.

(12) Kuang, P.; Hsieh, M.-L.; Lin, S.-Y. Integrated Three-Dimensional Photonic Nanostructures for Achieving Near-unity Solar Absorption and Superhydrophobicity. *J. Appl. Phys.* **2015**, *117*, 215309.

(13) Garnett, E.; Yang, P. Light Trapping in Silicon Nanowire Solar Cells. *Nano Lett.* **2010**, *10*, 1082−1087.

(14) Kelzenberg, M. D.; Turner-Evans, D. B.; Putnam, M. C.; Boettcher, S. W.; Briggs, R. M.; Baek, J. Y.; Lewis, N. S.; Atwater, H. A. High-performance Si Microwire Photovoltaics. *Energy Environ. Sci.* **2011**, *4*, 866−871.

(15) Zhu, J.; Yu, Z.; Burkhard, G. F.; Hsu, C.-M.; Connor, S. T.; Xu, Y.; Wang, Q.; McGehee, M.; Fan, S.; Cui, Y. Optical Absorption Enhancement in Amorphous Silicon Nanowire and Nanocone Arrays. *Nano Lett.* **2009**, *9*, 279−282.

(16) Lin, H.; Xiu, F.; Fang, M.; Yip, S.; Cheung, H. Y.; Wang, F.; Han, N.; Chan, K. S.; Wong, C. Y.; Ho, J. C. Rational Design of Inverted Nanopencil Arrays for Cost-Effective, Broadband, and Omnidirectional Light Harvesting. *ACS Nano* **2014**, *8*, 3752−3760.

(17) Mavrokefalos, A.; Han, S. E.; Yerci, S.; Branham, M. S.; Chen, G. Efficient Light Trapping in Inverted Nanopyramid Thin Crystalline Silicon Membranes for Solar Cell Applications. *Nano Lett.* **2012**, *12*, 2792−2796.

(18) Li, G.; Li, H.; Ho, J. Y. L.; Wong, M.; Kwok, H. S. Nanopyramid Structure for Ultrathin c-Si Tandem Solar Cells. *Nano Lett.* **2014**, *14*, 2563−2568.

(19) Zhou, L.; Yu, X.; Zhu, J. Metal-Core/Semiconductor-Shell Nanocones for Broadband Solar Absorption Enhancement. *Nano Lett.* **2014**, *14*, 1093−1098.

(20) Bermel, P.; Luo, C.; Zeng, L.; Kimerling, L. C.; Joannopoulos, J. D. Improving Thin-film Crystalline Silicon Solar Cell Efficiencies with Photonic Crystals. *Opt. Express* **2007**, *15*, 16986−17000.

(21) Chutinan, A.; John, S. Light Trapping and Absorption Optimization in Certain Thin-film Photonic Crystal Architectures. *Phys. Rev. A: At., Mol., Opt. Phys.* **2008**, *78*, 023825.

(22) Sheng, X.; Broderick, L. Z.; Kimerling, L. C. Photonic Crystal Structures for Light Trapping in Thin-film Si Solar Cells: Modeling, Process and Optimizations. *Opt. Commun.* **2014**, *314*, 41−47.

(23) Wang, K. X.; Yu, Z.; Liu, V.; Raman, A.; Cui, Y.; Fan, S. Light Trapping in Photonic Crystals. *Energy Environ. Sci.* **2014**, *7*, 2725−2738.

(24) Demésy, G.; John, S. Solar Energy Trapping with Modulated Silicon Nanowire Photonic Crystals. *J. Appl. Phys.* **2012**, *112*, 074326.

(25) Eyderman, S.; John, S.; Deinega, A. Solar Light Trapping in Slanted Conical-Pore Photonic Crystals Beyond Statistical Ray Trapping. *J. Appl. Phys.* **2013**, *113*, 154315.

(26) Frey, B. J.; Kuang, P.; Lin, S.-Y.; Jiang, J.-H.; John, S. Large-Scale Fabrication of a Simple Cubic Metal-Oxide Photonic Crystal for Light-Trapping Applications. *J. Vac. Sci. Technol. B* **2015**, *33*, 021804.

(27) Kuang, P.; Deinega, A.; Hsieh, M. L.; John, S.; Lin, S. Y. Light Trapping and Near-Unity Solar Absorption in a Three-Dimensional Photonic-Crystal. *Opt. Lett.* **2013**, *38*, 4200−4203.

(28) Eyderman, S.; John, S.; Hafez, M.; Al-Ameer, S. S.; Al-Harby, T. S.; Al-Hadeethi, Y.; Bouwes, D. M. Light-Trapping Optimization in Wet-Etched Silicon Photonic Crystal Solar Cells. *J. Appl. Phys.* **2015**, *118*, 023103.

(29) Biswas, R.; Sigalas, M. M.; Ho, K.-M.; Lin, S.-Y. Three-Dimensional Photonic Band Gaps in Modified Simple Cubic Lattices. *Phys. Rev. B: Condens. Matter Mater. Phys.* **2002**, *65*, 205121.

(30) Trompoukis, C.; Stesmans, A.; Simoen, E.; Depauw, V.; El Daif, O.; Lee, K.; Gordon, I.; Mertens, R.; Poortmans, J. Photonic Nanostructures for Advanced Light Trapping in Silicon Solar Cells: The Impact of Etching on The Material Electronic Quality. *Phys. Status Solidi RRL* **2016**, *10*, 158−163.

(31) Kerr, M. J.; Cuevas, A. Very Low Bulk and Surface Recombination in Oxidized Silicon Wafers. *Semicond. Sci. Technol.* **2002**, *17*, 35−38.

(32) Kerr, M. J.; Schmidt, J.; Cuevas, A.; Bultman, J. H. Surface Recombination Velocity of Phosphorus-Diffused Silicon Solar Cell Emitters Passivated with Plasma Enhanced Chemical Vapor Deposited Silicon Nitride and Thermal Silicon Oxide. *J. Appl. Phys.* **2001**, *89*, 3821−3826.

(33) Chen, M.; Chang, H.-C.; Chang, A. S.P.; Lin, S.-Y.; Xi, J.-Q.; Schubert, E. F. Design of Optical Path for Wide-Angle Gradient-Index Antireflection Coatings. *Appl. Opt.* **2007**, *46*, 6533−6538.

(34) Palik, E. D. *Handbook of Optical Constants of Solids*; Academic Press: San Diego, CA, 1998.

(35) Savin, H.; Repo, P.; von Gastrow, G.; Ortega, P.; Calle, E.; Garín, M.; Alcubilla, R. Black Silicon Solar Cells with Interdigitated Back-Contacts Achieve 22.1% Efficiency. *Nat. Nanotechnol.* **2015**, *10*, 624.

(36) Deinega, A.; Eyderman, S.; John, S. Coupled Optical and Electrical Modeling of Solar Cell Based on Conical Pore Silicon Photonic Crystals. *J. Appl. Phys.* **2013**, *113*, 224501.

(37) Green, M. A.; Keevers, M. J. Optical Properties of Intrinsic Silicon At 300 K. *Prog. Photovoltaics* **1995**, *3*, 189−192.

(38) Mallick, S. B.; Agrawal, M.; Peumans, P. Optimal Light Trapping in Ultra-Thin Photonic Crystal Crystalline Silicon Solar Cells. *Opt. Express* **2010**, *18*, 5691−5706.

(39) Green, M. A. Limits On the Open-Circuit Voltage and Efficiency of Silicon Solar Cells Imposed by Intrinsic Auger Processes. *IEEE Trans. Electron Devices* **1984**, *31*, 671−678.

(40) Shockley, W.; Queisser, H. J. Detailed Balance Limit of Efficiency of p-n Junction Solar Cells. *J. Appl. Phys.* **1961**, *32*, 510−519.